

RSC Advances



This is an *Accepted Manuscript*, which has been through the Royal Society of Chemistry peer review process and has been accepted for publication.

Accepted Manuscripts are published online shortly after acceptance, before technical editing, formatting and proof reading. Using this free service, authors can make their results available to the community, in citable form, before we publish the edited article. This *Accepted Manuscript* will be replaced by the edited, formatted and paginated article as soon as this is available.

You can find more information about *Accepted Manuscripts* in the [Information for Authors](#).

Please note that technical editing may introduce minor changes to the text and/or graphics, which may alter content. The journal's standard [Terms & Conditions](#) and the [Ethical guidelines](#) still apply. In no event shall the Royal Society of Chemistry be held responsible for any errors or omissions in this *Accepted Manuscript* or any consequences arising from the use of any information it contains.

Variable corrosion behavior of thick amorphous carbon coating in NaCl solution

Renhui Zhang^{a*}, Liping Wang^b, WeiShi^a

^aResearch Center of Material and Chemical Engineering, School of Material and Chemical Engineering, TongRen University, Tongren 554300, P. R. China

^bState Key Laboratory of Solid Lubrication, Lanzhou Institute of Chemical Physics, Chinese Academy of Science, Lanzhou 730000, China

Abstract: The present work investigated a thick amorphous multi-layer carbon coating fabricated by the plane hollow cathode plasma-enhanced chemical vapor deposition technique.. The thick amorphous multi-layer carbon coating included F-Si doped multi-layer structure and a silicon interlayer, which was able to reduce internal stress, improve the bonding and adhesion, and bridge the film and substrate. The work mainly discussed the cause of variable corrosion behaviors of the coating. Corrosion resistance was assessed by potentiodynamic polarization tests and electrochemical impedance spectroscopy (EIS) in 3.5 wt.% NaCl solution. The results showed that the mild electrochemical reactions and corrosion product film had a significant effect on dominating the variable corrosion behavior of the coating.

Keywords: Steel; EIS; Potentiodynamic polarization; DLC

* Corresponding author. Tel: +86 856-5592291.
E-mail address: zrh_111@126.com

1. Introduction

In the last few years, although the TiN, CrN and polymer could improve corrosion resistance of the substrate,[1-3] ultimately, they were prone to failure in the corrosive environments. However, diamond-like carbon (DLC) coatings have been extensively applied in electronic devices and vehicles due to their excellent corrosion resistance in corrosive environments.[4-12] It was well known that the corrosion resistance of DLC coatings was mainly determined by their chemical and physical properties.[13,14] Significant ways have been selected to improve the corrosion resistance of DLC coatings over the past years. For instance, incorporation of foreign atoms was treated as an effective way to increase the intrinsic properties of host materials. Thus, incorporation of foreign atoms into DLC coatings was potential candidates for improving the corrosion resistance of DLC coatings.[15,16] However, there were many aspects restricting the improvement of corrosion resistance of DLC coatings in corrosive medium. The defects, such as nano-pores, were the direct paths allowed the penetration of water, environmental oxygen and ions, corrosive media, which would lead to the electrochemical dissolution of the substrate.[4,17]

In addition, the corrosion resistance of DLC coatings could be well improved by increasing the thickness of the coatings.[10,18,19] Nevertheless there existed an inevitable inadequacy to be taken into account: internal stress would increase in in-situ deposition processes with increasing thickness of the coatings, which limited the coating thickness to a range between 1 and 3 μm ,[20] When the coating thickness more than 3 μm would result in cracking of the coatings from the substrate. Therefore,

reducing the nanopores and increasing the coating thickness were two keys to improve the corrosion resistance of the DLC coatings.

A possible method to well solve these problems through fabricating the multi-layer coating (MLCC) [21,22]. Since they could not only increase the thickness of the coatings, but also reduce the intrinsic internal stress and the possibility of through-coating defects.[20,23] Moreover, the MLCC containing the alternated interlayers and little nano-pores not only exhibited good corrosion resistance in corrosive solution due to its better possibilities of corrosion prevention,[24-26] but also low internal stress and high adhesion as reported our previous studies.[27,28] As we known, F or Si doped amorphous carbon coatings displayed the superior corrosion resistance in corrosive environments as reported by the most of previous studies.[29,30] Arguably, F and Si codoped amorphous carbon coatings should exhibit good corrosion resistance in corrosive environments. Therefore, to exploit a simple and durable MLCC would be desirable for improving the corrosion resistance of the amorphous carbon coating.

Herein, the objective of the present work was to fabricate a novel MLCC using the plane hollow cathode plasma-enhanced chemical vapor deposition technique, which should have aimed at improving corrosion resistance of the thick MLCC. Interestingly, the results of electrochemical tests showed that the coating exhibited the variable corrosion behavior in NaCl solution. The detailed discussion revealed that the variable corrosion behaviors were attributed to mild electrochemical reactions and corrosion product film.

2. Experimental procedure

Fig. 1a presents the schematic of the plane hollow cathode plasma-enhanced chemical vapor deposition system. Two, 7.5cm apart and stainless steel-made, parallel plates served as the electrode bodies, and the lower one also served as the substrate holder. The substrates used for coating deposition were AISI 304 stainless steel plates (30 mm × 30 mm × 1 mm) that were polished to a mirror finish. The stainless steel substrates were ultrasonically cleaned in acetone and alcohol for 30 min and dried by N₂ gas blowing. Then they were placed in a vacuum chamber and the chamber was pumped down to a pressure of 1.0×10^{-3} Pa using a composite molecular pump. The deposition process of the MLCC covered with DLC top-layer is shown in Fig. 1b. To grow these coatings, substrates were cleaned at a pressure of 1.5 Pa for 20 min with a constant flow of argon gas in order to remove the oxides. Then, a Si interlayer of about 0.2 ± 0.03 μm was deposited with SiH₄ gas of 50 sccm and Ar gas of 100 sccm (-15.0 kV bias voltage obtained from a high voltage power (voltage range: 0 to 20 kV), 15 Pa and 30% duty ratio) in order to improve the adhesion of the final coatings to the substrate. A multi-layer coating was deposited in a SiH₄, CF₄, C₂H₂ and Ar environment. The F_{x1}-Si_{y1}-DLC layers were deposited in SiH₄ (25 sccm), CF₄ (25 sccm), C₂H₂ (150 sccm) and Ar (100 sccm) at 4.0 Pa. The F_{x2}-Si_{y2}-DLC layers were deposited in SiH₄ (25 sccm), CF₄ (25 sccm), C₂H₂ (100 sccm) and Ar (100 sccm) at 2.8 Pa. Finally, pure DLC layer was deposited on the F-Si-DLC layers surface. Pure DLC layer was deposited from C₂H₂ (150 sccm) and Ar (100 sccm) gases by the same deposition system. The substrate bias voltage was maintained at -800 V derived from

low voltage power (voltage range: 0 to 1.5 kV), a duty cycle of 30%, and a repetition frequency at 1.5 kHz. No external heating of the substrate was employed, and the maximum temperature during deposition was about 180 °C.

The surface and fracture cross-sectional microstructure of the coating was obtained using a thermal field electron emission scanning electron microscope (JSM 6701F, FEI Quanta FEG 250). TEM images were examined in details by high-resolution transmission electron microscopy (HRTEM; TF20). The chemical composition of the coating was determined using time-of-flight elastic recoil detection analysis (TOF-ERDA). The chemical compositions of original coating and 5 mins of OCP test were examined using X-ray photoelectron spectroscopy (XPS : AXIS ULTRA^{DLD}). The residual stress was measured by stress-induced bending on an interferometer surface profiler. The curvature radii of the substrate before and after coating deposition was measured by the observation of Newton's rings using an optical interferometer system, and then the residual stress was calculated by the Stoney equation. The adhesion of the sample was tested by a scratch tester (CSEM Revetest) equipped with a diamond tip of radius 200 μm. The normal load was increased from 0 to 50 N at a loading rate of 50 N/min and a scratching speed of 10 mm/min. Electrochemical tests were carried out using a computer controlled potentiostat/frequency response analyzer (Autolab PGSTAT302N) to evaluate the corrosion behavior of bare and carbon coating coated AISI 304 stainless steel. A typical three electrode cell, consisting of the working electrode (0.5 cm² exposed area), saturated Ag/AgCl electrode (saturated with KCl) as reference electrode and platinum

as the counter electrode, was used in the corrosion tests. The corrosive medium was 3.5 wt.% NaCl solution. All the solutions prepared from deionized water with pH of around 6.8 ± 0.2 . Potentiodynamic polarization tests were carried out at scan rate of 0.5 mV/s from -160 mV with reference to open circuit potential (OCP) to a final anodic current density of 0.1 mA/cm^2 after an initial 30 min exposure to the test electrolyte for achieving a stabilized OCP.[31-33] Measurements of electrochemical impedance (EIS) were conducted at the open circuit potential with an AC amplitude of 10 mV after immersion of a sample into solution for 30 min. The frequency ranged from 0.01 Hz to 10^5 Hz.[34,35] The material used for this study was a commercial AISI 304 stainless steel. The chemical composition of which is listed in Table. 1. The data was reported by Dagbert.[36] The polarization resistance (R_p) values were then calculated using the following formula[37]:

$$R_p = \frac{\beta_a \beta_c}{2.33 i_{\text{corr}} (\beta_a + \beta_c)} \quad (1)$$

where R_p was in $\text{k}\Omega \text{ cm}^2$; β_a and β_c were in terms of mV/dec; and i_{corr} was in mA cm^{-2} .

Ahn described that the porosity of the protective coatings was an important factor for effective corrosion protection.[38] And the porosity of the protective coatings could be calculated according to Eq. (2).[39]

$$\alpha = \frac{R_{p(\text{substrate})}}{R_{p(\text{coating-substrate})}} \times 10^{-|\Delta E_{\text{corr}} / \beta_a|} \quad (2)$$

A quantitative measurement of the effect of defects (pores or pinholes) on coating density was the packing factor (P). According to the Ref. [37], the sum of the porosity

and the packing factor was 1.

3. Results

3.1. Microstructure and composition

The cross-sectional and surface morphologies of MLCC are illustrated in Figs. 2a and 2b. The typical cross-sectional morphology (Fig. 2a) reveals the coating with a total thickness of about $8 \pm 0.2 \mu\text{m}$, including a $0.2 \pm 0.03 \mu\text{m}$ silicon interlayer, $0.2 \pm 0.02 \mu\text{m}$ $\text{F}_{x1}\text{-Si}_{y1}\text{-DLC}$ layers, $0.5 \pm 0.04 \mu\text{m}$ $\text{F}_{x2}\text{-Si}_{y2}\text{-DLC}$ layers, $0.5 \pm 0.03 \mu\text{m}$ DLC layer. The surface morphology presented in Fig. 2b exhibits no micro-pores and cracks in the surfaces. In order to further investigate the microstructure of the coating, the TEM technique was utilized. Fig. 3a shows the TEM cross-sectional interface image of MLCC. It can be obviously observed that the compact multi-layer structure are found in the coating. Fig. 3b shows HRTEM image of coating surface, which exhibits an amorphous carbon network structure according to the SAED patterns.

The elemental depth profiling of the coating examined by TOF-ERDA is shown in Fig. 4. Only the six top layers (total thickness of $2 \mu\text{m}$) of the cyclical coating are detected due to the TOF-ERDA only getting a signal from the first 1 to $2 \mu\text{m}$ beneath the surface. The MLCC with top DLC layer consists of 7.95 at.% H, 0.11 at.% O, 1.46 at.% F, 0.78 at.% Si and the balance C. C is the major composition, indicating that it is a typical carbon coating. In scratch method, as shown in the typical scratch curve, the peeling-off value merely meant that the coating detached from the substrate, which was obviously adhesion failure mode.[40] Fig. 5 shows the typical scratch

curve of MLCC, the critical adhesion load is more than 20 N, indicating a good adhesion between coating and substrate, which is attributed to the low internal stress of the coating (about -0.5 GPa). The optical image (inset in Fig. 5) of the scratch trace for MLCC shows that no chipping is observed at the border of inside the scratch of MLCC until achieving the maximum load. The phenomenon suggests the exceptional adhesion between the coating and substrate.

3.2. Corrosion behavior

Fig. 6 shows the potentiodynamic polarization curves of AISI 304 stainless steel and simple DLC coating after 30 min exposures in 3.5 wt.% NaCl. Although the i_{corr} of the simple DLC coating is larger than that of bare 304 stainless steel, the value of E_{corr} of simple DLC coating exhibits more negative compared to the bare 304 stainless steel. Fig. 7 shows the SEM image of simple DLC coating after the potentiodynamic polarization test. The coating peels off the substrate after the potentiodynamic polarization test, which indicates the poor corrosion resistance of the simple DLC coating. Thus, in this work, we mainly discuss the corrosive behaviors of the thick multi-layer carbon coating. The open circuit potentials (E_{OC}) measured as a function of immersion time for the bare steel and thick multi-layer carbon coating are presented in Fig. 8. It is worth to note that the E_{OC} values for thick multi-layer coating are lower than those for the bare steel at 5 min of immersion in the 3.5 wt.% NaCl solution, then rapidly increase more positive than those for the bare steel. After 30 min of immersion, the E_{OC} values for thick multi-layer coating are more positive than those for the bare steel. Potentiodynamic polarization curves of AISI 304 stainless

steel and MLCC after 30 min exposures in 3.5 wt.% NaCl are presented in Fig. 9. The corrosion potential (E_{corr}) and the corrosion current density (i_{corr}) of the specimens derived from polarization curves are listed in Table 2. It can be seen that the E_{corr} and i_{corr} of 304 stainless steel is -0.149 V, 7.5×10^{-6} A cm^{-2} , respectively. For the MLCC, the E_{corr} (-0.133 V) shifts to the positive direction about 0.016 V and i_{corr} (5.1×10^{-9} A cm^{-2}) decreases by more than three orders of magnitude compared to the 304 stainless steel. The anodic (β_a) and cathodic (β_c) Tafel slopes are determined at the same time. Calculated polarization resistance (R_p) values are listed in Table 2. It is noted that the polarization resistance of MLCC increases by more than three orders of magnitude compared to the AISI 304 stainless steel. The large value of R_p corresponded to excellent corrosion resistance in potentiodynamic polarization test.[4] The potentiodynamic polarization test is a clear indication that the MLCC with top DLC layer displays superior corrosion resistance in 3.5 wt.% NaCl. In addition, the porosity and packing factor of the coating is computed according to Eq. (2) and the values are given in Table 2. The beneficial effects of greater packing factor acted on inhibiting the passage of the corroding solution to the substrate and reducing localized corrosion kinetics as declared by previous study.[37]

3.3. Electrochemical impedance spectroscopy

Electrochemical impedance spectroscopy (EIS) is employed to investigate the corrosion characteristics of AISI 304 stainless steel and MLCC in 3.5 wt.% NaCl solution. The resulting EIS plots of bare steel and MLCC are shown Fig. 10. Based on

the EIS plots, the appropriate equivalent circuits are proposed as shown in Fig. 11. R_s accounts for the solution resistance, R_i and R_{ct} can be assigned respectively to the pore resistance of the coating and the charge transfer resistance. CPE_1 and CPE_2 are the constant elements of the coating and electrical double layer (EDL), respectively. Constant phase elements are utilized here instead of pure capacitances because of the deviations from an ideal capacitive behavior. The CPE impedance may be calculated by:

$$Z_{CPE} = A(j\omega)^{-n} \quad (3)$$

where A was a constant and n was defined as the formula: [41]

$$n = 1 - 2\chi / 180 \quad (4)$$

where χ was the depression angle (in degrees) that evaluated the semicircle deformation. In many cases, this impedance element was introduced formally only for fitting impedance data. But the CPE behavior had sometimes been attributed to the fractal nature of the electrode interface.[42] The factor n , defined as a CPE power, was an adjustable parameter that always lied between 0.5 and 1. As $n = 1$, the CPE described an ideal capacitor. For $0.5 < n < 1$, the CPE described a distribution of dielectric relaxation times in frequency space, and when $n = 0.5$ the CPE represented a Warburg impedance with diffusion character.[43] Figs. 10a and 10b show the Nyquist diagrams for the MLCC and bare steel. It shows that the impedance values of multi-layer carbon coating are much larger than those for the bare steel. For multi-layer carbon coating, a high impedance modulus ($10^7 \Omega \cdot \text{cm}^2$) and two time constant is observed compared to the bare steel. Zhao et al reported that the semicircle

at the high frequencies indicated that the coating could be treated as a barriers to corrosive media.[44] Thus, the semicircle (Fig. 10a) at high frequencies revealed that the MLCC could function as barriers that made interfacial charge transfer difficult, Montemor et al[45] declared that the semicircle at high frequencies was characterized by a capacitive response. The corresponding Bode diagrams for MLCC are shown in Figs. 10c and 10d. In Fig. 10c, in the high frequency regions (10^3 to 10^5 Hz), the relationship between impedance and frequency is almost linear with a slope close to -1 . This capacitive behavior is related to the EDL at the corrosive solution/coating interface. The phase angle Bode plots in Fig. 10d show a capacitive response in the high frequency domain, which could be linked to the barrier properties of the multi-layer carbon coating.[46] There is a resistance response in the low frequency range, which is a consequence of formation of conductive pathways through the coating. Table 3 shows the impedance parameters of corresponding equivalent circuits to fit the impedance data of 304 stainless steel and MLCC after being exposed in 3.5 wt.% NaCl. The larger values of R_{ct} and R_i had been conducive to improving the resistance to corrosion and decrease the corrosion rate.[5,47] The consequences of EIS tests are well consistence with that obtained results from potentiodynamic polarization tests.

The corroded surface (0.5 cm^2 area) of MLCC after EIS tests in 3.5 wt. % NaCl is shown in Fig. 12. The high magnification SEM image depicted in Fig. 12a shows that no evident corrosion damages are found on MLCC surface, and the coating has not been decomposed attributing to the strong adhesion between coating and substrate.

The EDS analysis is carried out at the region in Fig. 12b and the results (Figs. 12c-12g) show that the materials on the coating surface mainly consist of C, Na and Cl, indicating that the coating provides superior protection to the steel substrate in a short term.

3.4. Long-term electrochemical impedance spectroscopy

Generally, the corrosion behavior of the coating obtained from short-term EIS tests does not well illustrate that the coating is really good or bad corrosion resistance in corrosive environments. Accordingly, the long-term EIS tests are supposed to further understand the corrosion behavior of MLCC. EIS diagrams with the bare steel and multi-layer carbon coating obtained at different times of immersion in 3.5 wt.% NaCl are presented in Figs. 13 and 14. For the bare steel (Fig. 13), a low impedance modulus ($10^3 \text{ k}\Omega\cdot\text{cm}^2$) and only one time constant is observed throughout the plot, which is attributed to the formation of passivating film. The increment of corrosion resistance of the bare steel was ascribed to the passivating film.[48] For multi-layer carbon coating (Fig. 14), the total impedance of the system is above $10^4 \text{ k}\Omega\cdot\text{cm}^2$, being independent on the immersion time. In the low frequency regions (Figs. 14a and 14b), the linear part, due to control of the diffusion process, has a particularity for the multi-layer carbon coating coated work electrode. At the initial 2.5 h of immersion, the plot reveals a capacitive response in the high frequency domain, which could be related to the barrier properties of the multi-layer carbon coating.[49] In the low frequency regions, there is a resistance response, which is a consequence of formation of conductive pathways through the coating. Fe is detected on the coating surface,

indicating the occurrence of mild corrosion reactions between corrosive solution and substrate, as shown in Fig. 15. It suggests that the corrosion processes occur in the amorphous carbon coating coated steel substrate. As the immersion time elapsed, after 32.5 h of immersion, all the spectra present similar behavior, showing that the impedance values are almost constant.

For multi-layer carbon coating, although the overall process is expected to be dynamic, a single circuit can be used as the EIS response depends upon the presence of immersion time. For the equivalent circuits depicted in Fig. 16, R_s is the solution resistance, R_f represents the passivating film resistance, R_i is suggested to represent the pore resistance, and R_{pf} is the corrosion products film resistance. CPE_0 , CPE_1 and CPE_2 are the constant elements of the passivating film, multi-layer carbon coating and corrosion products film, respectively. W_0 is a Warburg element, producing a Warburg impedance, R_w . Warburg element W_0 represented the linear diffusion to the reduced electrode surface.[49,50] The circuit elements calculated from the fitting results of the bare steel and MLCC are summarized in Table 4 and 5, respectively. Interestingly, from Table 5, in the range from 2.5 to 12.5 h of immersion, the decrease of the R_i of the multi-layer carbon coating resulted from the increase of immersion time due to the formation and growth of new pores.[51] While beyond 12.5 h of immersion, the R_i increases to a maximum value of $49.7 \text{ k}\Omega\cdot\text{cm}^2$ and the R_{pf} still remains a high value in Table 5, which was attributed to the compact structure allowing the corrosion products to plug the micro-corrosion holes more efficiently,[52] as can be seen in Fig. 15. Importantly, the coating is closely adhesive to the steel substrate, as shown in Fig.

17.

4. Discussion

A multi-layer amorphous carbon coating is successfully fabricated using a simple deposition technique. Generally, a multi-layer carbon coating could be expected to improve the corrosion resistance due to: (a) increasing coating thickness, which statistically reduces the possibility of through-coating defects such as pores; (b) alternating interlayers leading to different electrical behavior, which could redirect the current flow between coating and substrate, as reported by the most of previous investigations.[23,24] In this paper, the thick multi-layer carbon coating exhibits the variable corrosion behavior. The interesting corrosion behaviors are well discussed as follows.

The OCP of the thick multi-layer carbon coating exhibits the variable behavior. We analyze the chemical composition of the coating after 5 mins OCP test. Fig. 18 shows that the (a) XPS C 1s and (b) Si 2p spectra of original coating and 5 mins of OCP test. Fig. 18a shows that the intensity of C1s spectra decreases after 5 mins of OCP test, but the composition did not change. Fig. 18b exhibits that the intensity of Si 2p spectra changes from the low value to the large one after 5 mins of OCP test. Moreover, the Si-O and Si-C bonds group sharply increase after 5 mins of OCP test. Bunker et al [25] reported that the relative reactivities of strained and unstrained Si-O bonds show that bond strain promoted bond rupture reactions that led to stress corrosion cracking. Thus, the potential drop at ~5 mins of OCP test for thick

multi-layer carbon coating should be attributed to this reason. In addition, Maguire [26] reported that amorphous carbon film containing Si-C bonds could exhibit good corrosion resistance. Thus, the increase in potential after 5 mins of OCP test could be attributed to the effect of Si-C bonds.

The alternated interlayer structures are found in the multi-layer amorphous carbon coating as shown in Figs. 2a and 3a. As reported in our previous investigations,[27,28] this structure could improve adhesion load between coating and substrate and reduce internal stress of the coating. Reducing internal stress and increasing adhesion force was an effective approach to improve the resistance to corrosion.[53-57] Based on these literatures survey, in this investigation, the amorphous carbon coating containing F-Si-doped multi-layer structure and possessing low internal stress (-0.5 GPa) and high critical load (>20 N) should exhibit good corrosion resistance in 3.5 wt.% NaCl solution. However, Fig. 14 shows that after immersion of 2.5 h, the corrosion resistance of the thick multi-layer carbon coating tends to gradually decrease. As described in Fig. 15, Fe and small corrosion products are detected on the coating surface, indicating that mild corrosion reactions are observed in amorphous carbon coating coated steel immersion of 2.5 h in 3.5 wt.% NaCl solution. We can therefore conclude that the decrease of corrosion resistance could be attributed to the mild corrosion reactions. It can also be seen from Fig. 17 that the coating does not peel off from the substrate, indicating well adhesion between coating and substrate. Thus, the mild corrosion reactions would be one of the reasons that lead to the variable corrosion behaviors.

In addition, corroding solution penetration generally took place through real microscopic pores and virtual pores, which were regions of low cross-linking, and therefore high transport. A highly dense cross-linked structure made the multi-layer carbon coating less permeable to the corrosive medium leading to less delamination along the coating/substrate interface, since the coating was less permeable, as reported by Liu.[20] The multi-layer carbon coating possesses high value of packing factor (Table 2), thus, in the absence of macroscopic pores or other easily accessible defects for the corroding solution, the pore resistance R_i originates from the actual ionic conductivity of the multi-layer carbon coating. Papakonstantinou reported that the high value of pore resistance R_i of a DLC film reflected the large degree to which the film formed a barrier that hinders electrolytic conduction.[5] In the range from 2.5 to 12.5 h, the decrease of R_i indicated the formation and growth of new pores, as reported by Zheludkevich.[51] However, in the range from 17.5 to 32.5 h, the decrease of R_i indicates that the ability of inhibiting the corroding solution becomes weak. Nevertheless, the coating still displayed good corrosion resistance after the immersion time beyond 12.5 h, which was attributed to the compact structure of the coating allowing the corrosion rust to plug the micro-corrosion holes more efficiently,[52] leading to high R_{pf} values (Table 5) that could still improve the corrosion resistance of the coating. Thus, the above observation and discussion brings out clearly the fact that the corrosion product film has a significant effect on the corrosion resistance of the coating in 3.5 wt.% NaCl solution, which could be another reason for the variable corrosion behaviors

5. Conclusions

The simple DLC coating and thick multi-layer carbon coating is successfully fabricated by a plane hollow cathode plasma-enhanced chemical vapor deposition method. Compared to simple DLC coating, the thick multi-layer carbon coating exhibits good corrosion resistance. Interestingly, the EIS results of thick multi-layer carbon coating demonstrate that the thick multi-layer carbon coating exhibits the variable corrosion behaviors in 3.5 wt.% NaCl solution. The variable corrosion behaviors are discussed in details, which shows that the variable corrosion behaviors are attributed to the effect of the mild electrochemical reactions and corrosion product film.

References

- [1] Bayón R, Igartua A, Fernández X, Martínez R, Rodríguez RJ, García JA, De Frutos A, Arenas MA, De Damborenea J, Corrosion-wear behaviour of PVD Cr/CrN multilayer coatings for gear applications. (2009) *Tribol. Int.* 42:591–599.
- [2] Major L, Lackner JM, Major B, Bio-tribological TiN/Ti/aC:H M\multilayer coatings development with built-in mechanism of controlled wear. (2014) *RSC Adv.* 4:21108–21114.
- [3] Zhu J, Wei S, Lee IY, Park S, Wills J, Haldolaarachchiq N, Young DP, Luo ZP, Guo ZH, Silica stabilized iron particles toward anti-corrosion magnetic polyurethane nanocomposites. (2012) *RSC Adv.* 2:1136–1143.
- [4] Khun NW, Liu E, Zeng XT, Corrosion behavior of nitrogen doped diamond-like

carbon thin films in NaCl solutions. (2009) *Corros. Sci.* 51: 2158.

[5] Papakonstantinou P, Zhao JF, Lemonine P, McAdams ET, McLaughlin JA, The effects of Si incorporation on the electrochemical and nanomechanical properties of DLC thin films. (2002) *Diamond Relat. Mater.* 11: 1074.

[6] Kim HG, Ahn SH, Kim JG, Park SJ, Lee KR, Corrosion performance of diamond-like carbon (DLC)-coated Ti alloy in the simulated body fluid environment. (2005) *Diamond Relat. Mater.* 14:53.

[7] Zeng A, Liu E, Tan SN, Zhang S, Gao J, Cyclic voltammetry studies of sputtered nitrogen doped diamond-like carbon film electrodes. (2002) *Electroanalysis* 14:1110.

[8] Cai W, Sui JH, Effect of working pressure on the structure and the electrochemical corrosion behavior of diamond-like carbon (DLC) coatings on the NiTi alloys. (2007) *Surf. Coat. Technol.* 201:5194.

[9] Liu CL, Hu DP, Xu J, Yang DZ, Qi M, In vitro electrochemical corrosion behavior of functionally graded diamond-like carbon coatings on biomedical Nitinol alloy. (2006) *Thin Solid Films* 496: 457.

[10] Sharma R, Barhai PK, Kumari N, Corrosion resistant behaviour of DLC films. (2008) *Thin Solid Films* 516:5397.

[11] Kim HG, Ahn SH, Kim JG, Park SJ, Lee KR Electrochemical behavior of diamond-like carbon films for biomedical applications. (2005) *Thin Solid Films* 475: 291.

[12] Liu E, Kwek HW, Electrochemical performance of diamond-like carbon thin films. (2008) *Thin Solid Films* 516:5201.

- [13] Liu LX, Liu E, Nitrogenated diamond-like carbon films for metal tracing. (2005) Surf. Coat. Technol. 198:189.
- [14] Zeng A, Liu E, Annergren IF, Tan SN, Zhang S, Hing P, Gao J, EIS capacitance diagnosis of nanoporosity effect on the corrosion protection of DLC films. (2002) Diamond Relat. Mater. 11:160.
- [15] Trippe SC, Pereira L, Electrical and photocurrent analysis of Si–fluorine doped DLC films heterojunctions. (2007) Diamond Relat. Mater. 16:1349.
- [16] Dai W, Wu GS, Wang AY, Preparation Preparation, characterization and properties of Cr-incorporated DLC films on magnesium alloy. (2010) Diamond Relat. Mater. 19:1307.
- [17] Song GH, Yang XP, Xiong GL, Lou Z, Chen LJ, The corrosive behavior of Cr/CrN multilayer coatings with different modulation periods. (2013) Vacuum 89: 136–141.
- [18] Dorner-Reisel A, Schürer C, Irmer G, Müller E, Electrochemical corrosion behaviour of uncoated and DLC coated medical grade $\text{Co}_{28}\text{Cr}_6\text{Mo}$. (2004) Surf. Coat. Technol. 177: 830–873.
- [19] Hadinata SS, Lee MT, Pan SJ, Tsai WT, Tai CY, Shih CF, Electrochemical performances of diamond-like carbon coatings on carbon steel, stainless steel and brass. (2013) Thin Solid Films 529:412–416.
- [20] Xu Z, Zheng YJ, Liang F, Leng YX, Sun H, Huang N, The microstructure and mechanical properties of multilayer diamond-like carbon films with different modulation ratios. (2013) Appl. Surf. Sci. 264:207–212.

- [21] Uematsu Y, Kakiuchi T, Teratani T, Harada Y, Tokaji K, Improvement of corrosion fatigue strength of magnesium alloy by multilayer diamond-like carbon coatings. (2011) *Surf. Coat. Technol.* 205:2778–2784.
- [22] Feng K, Li Z, Lu F, Huang J, Cai X, Wu Y, Corrosion resistance and electrical properties of carbon/chromium–titanium–nitride multilayer coatings on stainless steel. (2014) *J. Power Sources* 249:299–305.
- [23] Liu C, Leyland A, Bi Q, Matthews A, Corrosion resistance of multi-layered plasma-assisted physical vapour deposition TiN and CrN coatings. (2001) *Surf. Coat. Technol.* 141:164–173.
- [24] Dobrzański LA, Lukaszewicz K, Pakula D, Mikula J, Corrosion resistance of multilayer and gradient coatings deposited by PVD and CVD techniques. (2007) *Arch. Mater. Sci. Eng* 28:12.
- [25] Härkönen E, Kolev I, Díaz B, Światowska J, Maurice V, Seyeux A, Marcus P, Fenker M, Toth L, Radnoczi G, Vehkamäki M, Ritala M, Sealing of Hard CrN and DLC Coatings with Atomic Layer Deposition. (2014) *ACS Appl. Mater. Interfaces* 6 :1893.
- [26] Liu CL, Yang DZ, Lin GQ, Qi M, Corrosion resistance and hemocompatibility of multilayered Ti/TiN-coated surgical AISI 316L stainless steel. (2005) *Mater. Lett.* 59:3813.
- [27] Wang JJ, Pu JB, Zhang GA, Wang LP, Interface architecture for superthick carbon-based films toward low internal stress and ultrahigh load-bearing capacity. (2013) *ACS Appl. Mater. Inter.* 5:5015.

- [28] Wang JJ, Pu JB, Zhang GA, Wang LP, Tailoring the structure and property of silicon-doped diamond-like carbon films by controlling the silicon content. (2013) *Surf. Coat. Technol.* 59:312.
- [29] Marciano FR, Almeida EC, Lima-Oliveira DA, Corat EJ, Trava-Airoldi VJ, Improvement of DLC electrochemical corrosion resistance by addition of fluorine, (2010) *Diamond Relat. Mater.* 19:537.
- [30] Sui JH, Zhang ZG, Cai W, Surface characteristics and electrochemical corrosion behavior of fluorinated diamond-like carbon (F-DLC) films on the NiTi alloys. (2009) *Nucl. Instrum. Meth. B* 267:2475.
- [31] Liang J, Srinivasan PB, Blawert C, Dietzel W, Influence of chloride ion concentration on the electrochemical corrosion behaviour of plasma electrolytic oxidation coated AM50 magnesium alloy. (2010) *Electrochim. Acta* 55:6802.
- [32] Zhang RH, Liang J, Wang Q, Preparation and characterization of graphite-dispersed styrene-acrylic emulsion composite coating on magnesium alloy. (2012) *Appl. Surf. Sci.* 258: 4360.
- [33] Wang LP, Lin YL, Zeng ZX, Liu WM, Xue QJ, Hu LT, Zhang JY, Electrochemical corrosion behavior of nanocrystalline Co coatings explained by higher grain boundary density. (2007) *Electrochim. Acta* 52 :4342.
- [34] Liang J, Srinivasan PB, Blawert C, Dietzel W, Comparison of electrochemical corrosion behaviour of MgO and ZrO₂ coatings on AM50 magnesium alloy formed by plasma electrolytic oxidation. (2009) *Corros. Sci.* 51:2483.
- [35] Wang LP, Zhang JY, Gao Y, Xue QJ, Hu LT, Xu T, Grain size effect in corrosion

behavior of electrodeposited nanocrystalline Ni coatings in alkaline solution. (2006)

Scripta Mater. 55:657.

[36] Dagbert C, Meylheuc T, Bellon-Fontaine MN, Corrosion behaviour of AISI 304 stainless steel in presence of a biosurfactant produced by *Pseudomonas fluorescens*. (2006) *Electrochim. Acta* 51(24):5221.

[37] Chang ZT, Cherry B, Marosszeky M, Polarisation behaviour of steel bar samples in concrete in seawater. Part 2: A polarisation model for corrosion evaluation of steel in concrete. (2008) *Corros. Sci.* 50:3078.

[38] Ahn SH, Lee JH, Kim JG, Han JG, Localized corrosion mechanisms of the multilayered coatings related to growth defects. (2004) *Surf. Coat. Technol.* 177-178: 638.

[39] Matthes B, Broszeit E, Aromaa J, Ronkainen H, Hannula SP, Leyland A, Matthews A, Corrosion performance of some titanium-based hard coatings. (1991) *Surf. Coat. Technol.* 49:489.

[40] Cheng K, Ren CB, Weng WJ, Du PY, Shen G, Han GR, Zhang S, Bonding strength of fluoridated hydroxyapatite coatings: a comparative study on pull-out and scratch analysis. (2009) *Thin Solid Films* 517:5361.

[41] Flis J, Tobiyama Y, Mochizuki K, Chiga C, Characterisation of phosphate coatings on zinc, zinc-nickel and mild steel by impedance measurements in dilute sodium phosphate solutions. (1997) *Corros. Sci.* 39:1757.

[42] Jimenez-Morales A, Galvan JC, Rodriguez R, De JJ, Damborena Electrochemical study of the corrosion behaviour of copper surfaces modified by nitrogen ion

implantation. (1997) *J. Appl. Electrochem.* 27:550.

[43] Martini EMA, Muller IL, Characterization of the film formed on iron in borate solution by electrochemical impedance spectroscopy. (2000) *Corros. Sci.* 42: 443.

[44] Zhao G, Feng JJ, Xu JJ, Chen HY, Direct electrochemistry and electrocatalysis of heme proteins immobilized on self-assembled ZrO₂ film. (2005) *Electrochem. Commun.* 7:724.

[45] Montemor MF, Trabelsi W, Zheludevich M, Ferreira MGS, Modification of bis-silane solutions with rare-earth cations for improved corrosion protection of galvanized steel substrates. (2006) *Prog. Org. Coat.* 57: 67.

[46] Taryba M, Lamaka SV, Snihirova D, Ferreira MGS, Montemor MF, Wijting WK, Toews S, Grundmeier G, The combined use of scanning vibrating electrode technique and micro-potentiometry to assess the self-repair processes in defects on “smart” coatings applied to galvanized steel. (2011) *Electrochim. Acta* 56:4475.

[47] Xiao Z, Li Z, Zhu AY, Zhao YY, Chen JL, Zhu YT, Surface characterization and corrosion behavior of a novel gold-imitation copper alloy with high tarnish resistance in salt spray environment. (2013) *Corros. Sci.* 76:42.

[48] Okamoto G, Passive film of 18-8 stainless steel structure and its function. (1973) *Corros. Sci.* 13:471.

[49] Posudievsky OY, Kozarenko OA, Dyadyun VS, Jorgensen SW, Spearot JA, Koshechko VG, Pokhodenko VD, Effect of host-guest versus core-shell structure on electrochemical characteristics of vanadium oxide/polypyrrole nanocomposites. (2011) *Electrochim. Acta* 58:442.

- [50] Casero E, Parra-Alfambra AM, Petit-Domínguez MD, Pariente F, Lorenzo E, Alonso C, Differentiation between graphene oxide and reduced graphene by electrochemical impedance spectroscopy (EIS). (2012) *Electrochem. Commun.* 20: 63.
- [51] Zheludkevich ML, Serra R, Montemor MF, Yasakau KA, Salvado IMM, Ferreira MGS, Nanostructured sol–gel coatings doped with cerium nitrate as pre-treatments for AA2024-T3: Corrosion protection performance. (2005) *Electrochim. Acta* 51:208.
- [52] Liu CL, Chu PK, Lin GQ, Yang DZ, Effects of Ti/TiN multilayer on corrosion resistance of nickel-titanium orthodontic brackets in artificial saliva. (2007) *Corros. Sci.* 49:3783.
- [53] Choi J, Nakao S, Kim J, Ikeyama M, Kato T, Corrosion protection of DLC coatings on magnesium alloy. (2007) *Diamond Relat. Mater.* 16:1361.
- [54] Yasuda HJ, Plasma polymerization first ed., Academic Press, New York, 1985.
- [55] Rangel RCC, Souza MEP, Schreiner WH, Freire CMA, Rangel EC, Cruz NC, Effect of the fluorination of DLC film on the corrosion protection of aluminum alloy (AA 5052). (2010) *Surf. Coat. Technol.* 204:3022.
- [56] Wu GS, Sun LL, Dai W, Song LX, Wang AY, Influence of interlayers on corrosion resistance of diamond-like carbon coating on magnesium alloy. (2010) *Surf. Coat. Technol.* 204:2193.
- [57] Fenker M, Balzer M, Jehn HA, Kappl H, Lee JJ, Lee KH, Park HS, Improvement of the corrosion resistance of hard wear resistant coatings by intermediate plasma etching or multilayer structure. (2002) *Surf. Coat. Technol.*

150:101.

Figure.1 Schematic of (a) the PECVD deposition system and (b) deposition process using hollow cathode effect.

Figure 2. (a) SEM cross-sectional image of thick multi-layer carbon coating. (b) Surface morphology of thick multi-layer carbon coating.

Figure 3. (a) The TEM image of interface morphology of thick multi-layer carbon coating. (b) High resolution TEM (HRTEM) image of the surface morphology of thick multi-layer carbon coating (inset is SAED pattern).

Figure 4. Elemental depth profiling of thick multi-layer carbon coating examined by TOF-ERDA.

Figure 5. The scratch curve of thick multi-layer carbon coating.

Figure 6. Open circuit potential vs. immersion time in 3.5 wt.% NaCl solution for bare steel and thick multi-layer carbon coating.

Figure 7. Potentiodynamic polarization curves for 304 stainless steel and simple DLC coating in 3.5 wt.% NaCl.

Figure 8. The SEM image of simple DLC coating after the potentiodynamic polarization test in 3.5 wt.% NaCl.

Figure 9. Potentiodynamic polarization curves for 304 stainless steel and thick multi-layer carbon coating in 3.5 wt.% NaCl.

Figure 10. Experimental (a) and (b) Nyquist and (c) and (d) Bode plots of 304 stainless steel and thick multi-layer carbon coating in 3.5 wt.% NaCl solution.

Figure 11. The equivalent circuits used to fit the impedance data of (a) the bare steel

and (b) thick multi-layer carbon coating in 3.5 wt.% NaCl solution.

Figure 12. Surface appearances of thick multi-layer carbon coating in 3.5 wt.% NaCl solution: (a) high magnification SEM morphology of thick multi-layer carbon coating; (b) high magnification SEM image showing the localized corrosion of the thick multi-layer carbon coating. The elemental EDS maps are taken from the whole areas shown in Fig. 10b are shown for (c) C K, (d) Si K, (e) F K, (f) Cl K, (g) Na K.

Figure 13. EIS plots (experimental) and the fitting curves (solid lines) for bare steel (a) Nyquist plots, (b) and (c) Bode plots at different times of immersion in 3.5 wt.% NaCl.

Figure 14. EIS plots (experimental) and the fitting curves (solid lines) for thick multi-layer carbon coating (a) and (b) Nyquist plots, (b) and (c) Bode plots at different times of immersion in 3.5 wt.% NaCl.

Figure 15. (a) Secondary electron (SEI) of the surface of the thick multi-layer carbon coating for immersion 2.5 h in 3.5 wt.% NaCl. (b) high magnification SEM image showing the localized corrosion of the thick multi-layer carbon coating. The elemental EDS maps are taken from the whole areas shown in Fig. 13b are shown for (c) Cl K, (d) C K, (e) Si K, (f) F K, (g) Fe K, (H) Na K.

Figure 16. The equivalent electrical circuits for the impedance plots fitting of (a) the bare steel, (b) thick multiple-layer carbon coating immersion in 3.5 wt.% NaCl.

Figure 17. The SEM image between the coating and steel substrate after immersion of 32.5 h.

Figure 18. The XPS (a) C 1s and (b) Si 2p spectra for original coating and 5 mins of

OCP test.

Table 1 The chemical composition (% weight) of AISI 304 stainless steel.

Composition	C	Cr	Ni	Mn	N	S	Fe
wt. %	0.047	18.27	8.66	1.19	0.078	0.0007	Balance

Table 2 Results of porosity and packing factor obtained from electrochemical experiments.

Specimen	E_{corr} (V)	i_{corr} (A cm^{-2})	β_a (V dec^{-1})	β_c (V dec^{-1})	R_p ($\Omega \text{ cm}^2$)	Porosity (α)	Packing Factor (P)
Steel	-0.149	7.5×10^{-6}	0.418	0.354	1.1×10^4	–	–
Thick multiple-layer carbon coating	-0.133	5.1×10^{-9}	0.128	3.6	1.1×10^7	0.00078	0.99922

Table 3 Equivalent circuit data of the thick multi-layer carbon coating and 304 stainless steel in 3.5 wt.% NaCl solution. The respective fitting parameters obtained using ZView2.

	$CPE_1\text{-P}$ or n_1	$CPE_1\text{-T}$ ($\text{F}\cdot\text{cm}^{-2}\cdot\text{s}^{(n-1)}$)	R_i ($\Omega\cdot\text{cm}^2$)	$CPE_2\text{-P}$ or n_2	$CPE_2\text{-T}$ ($\text{F}\cdot\text{cm}^{-2}\cdot\text{s}^{(n-1)}$)	R_{ct} ($\Omega\cdot\text{cm}^2$)
304 stainless steel	–	–	–	0.84	2.4×10^{-5}	4.8×10^3
Thick multiple-layer carbon coating	0.68	7.1×10^{-8}	3.4×10^6	0.98	4.0×10^{-7}	3.1×10^8

Table 4 EIS parameters corresponding to the equivalent circuit for the bare steel in 3.5 wt.% NaCl after different times of immersion at open circuit potential. The respective fitting parameters obtained using ZView2.

Time of immersion, hours	$CPE_0\text{-P}$ or n_0	$CPE_0\text{-T}$ ($\text{F}\cdot\text{cm}^{-2}\cdot\text{s}^{(n-1)}$)	R_f ($\Omega\cdot\text{cm}^2$)	$CPE_2\text{-P}$ or n_2	$CPE_2\text{-T}$ ($\text{F}\cdot\text{cm}^{-2}\cdot\text{s}^{(n-1)}$)	R_{ct} ($\Omega\cdot\text{cm}^2$)
2.5	0.85	5.9×10^{-6}	1.4×10^4	0.54	6.1×10^{-6}	3.7×10^6
7.5	0.82	7.0×10^{-6}	2.22×10^5	0.71	7.7×10^{-6}	1.4×10^6
12.5	0.83	5.0×10^{-6}	3.83×10^5	0.63	5.3×10^{-6}	5.2×10^7
17.5	0.83	5.3×10^{-6}	2.5×10^5	0.73	5.5×10^{-6}	2.4×10^6
22.5	0.84	5.1×10^{-6}	2.25×10^5	0.74	5.2×10^{-6}	2.3×10^6

27.5	0.88	2.9×10^{-6}	7.45×10^4	0.54	3.0×10^{-6}	5.2×10^7
32.5	0.89	2.5×10^{-6}	5.0×10^3	0.55	2.7×10^{-6}	2.4×10^7

Table 5 EIS parameters corresponding to the equivalent circuit for thick multiple-layer carbon coating in 3.5 wt.% NaCl after different times of immersion at open circuit potential. The respective fitting parameters obtained using ZView2.

Time of immersion, hours	CPE_{1-P}	CPE_{1-T}	R_i	CPE_{3-P}	CPE_{3-T}	R_{pf}	R_w
	or n_1	($F \cdot cm^{-2} \cdot s^{(n-1)}$)	($\Omega \cdot cm^2$)	or n_3	($F \cdot cm^{-2} \cdot s^{(n-1)}$)	($\Omega \cdot cm^2$)	($\Omega \cdot cm^2$)
2.5	0.94	2.4×10^{-9}	2.02×10^4	0.64	2.8×10^{-8}	2.9×10^6	6.6×10^5
7.5	0.95	2.2×10^{-9}	5.5×10^3	0.63	9.8×10^{-8}	3.8×10^6	5.5×10^5
12.5	0.98	9.4×10^{-11}	1.4×10^3	0.66	9.5×10^{-8}	2.9×10^6	1.9×10^6
17.5	0.76	2.7×10^{-8}	4.97×10^4	0.63	9.7×10^{-8}	3.1×10^6	1.8×10^6
22.5	0.83	1.2×10^{-8}	1.55×10^4	0.64	1.5×10^{-7}	2.4×10^6	7.0×10^6
27.5	0.82	1.2×10^{-8}	1.27×10^4	0.64	1.7×10^{-7}	3.2×10^3	3.9×10^6
32.5	0.89	4.8×10^{-9}	3.0×10^3	0.66	1.8×10^{-7}	3.5×10^6	7.4×10^3

Figure 1

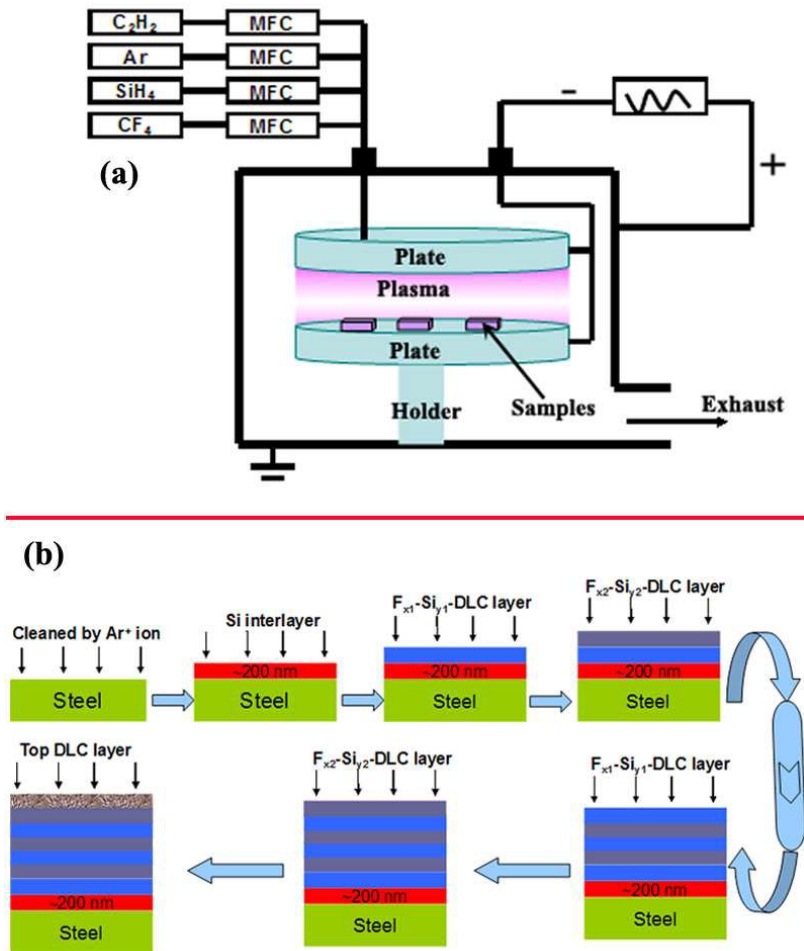


Figure 2

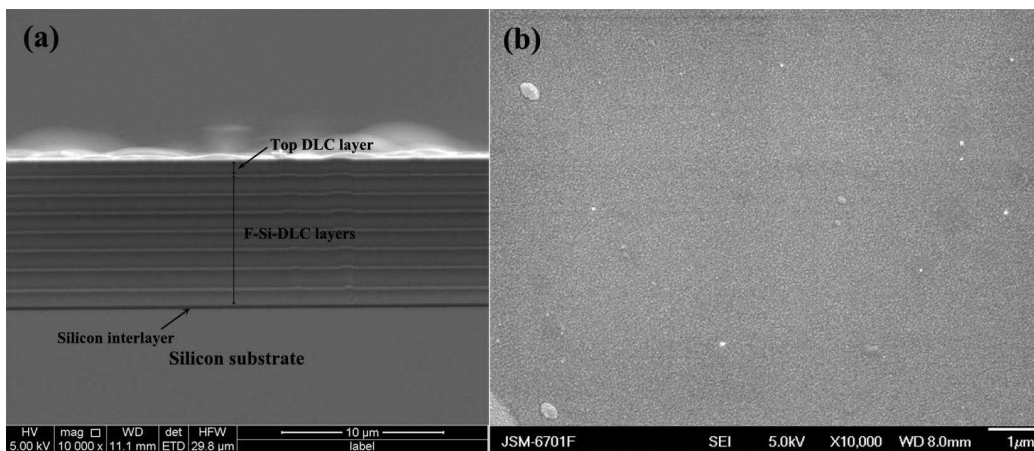


Figure 3

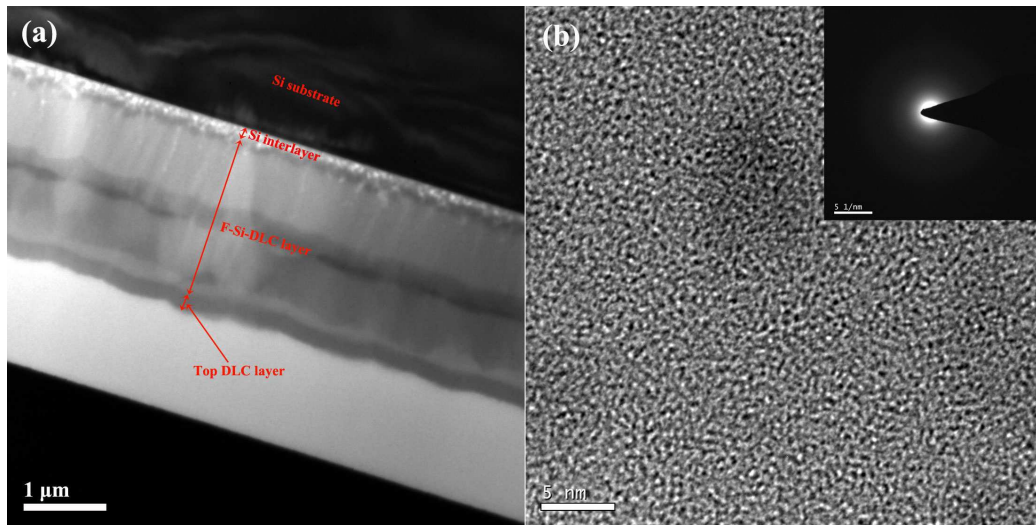


Figure 4

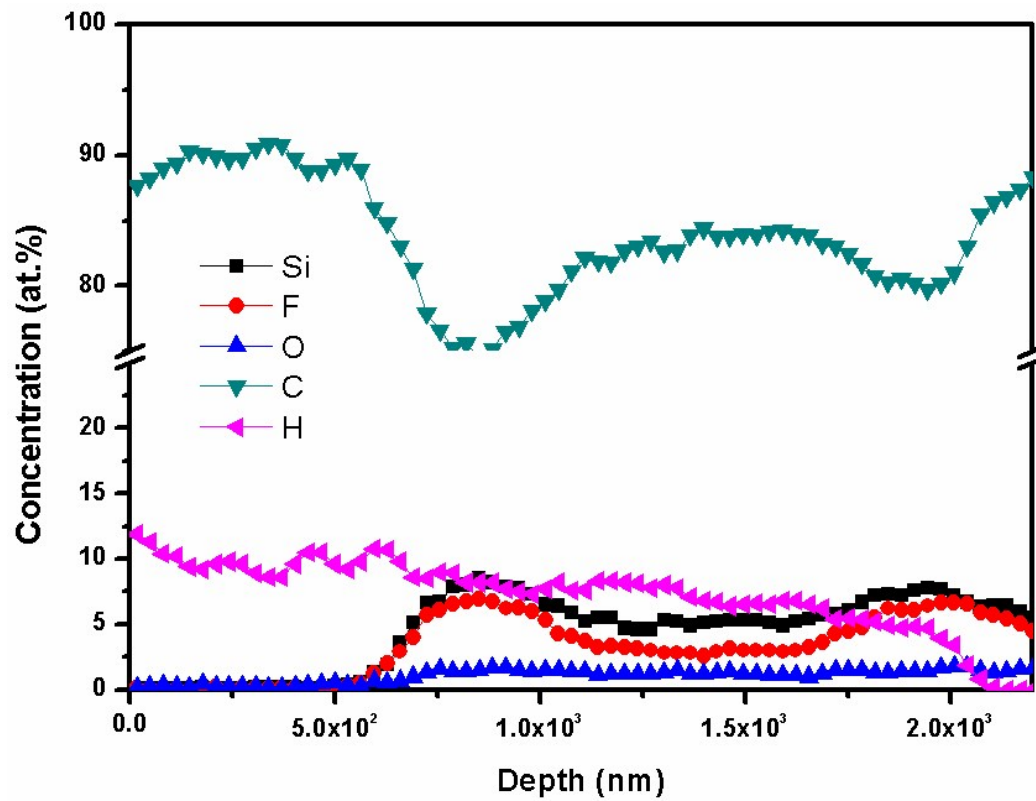


Figure 5

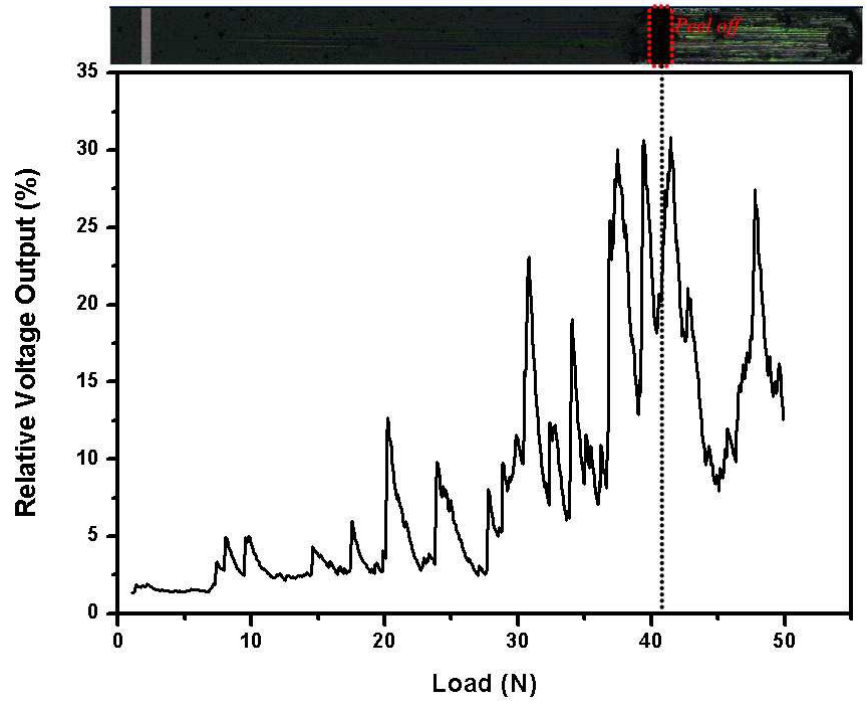


Figure 6

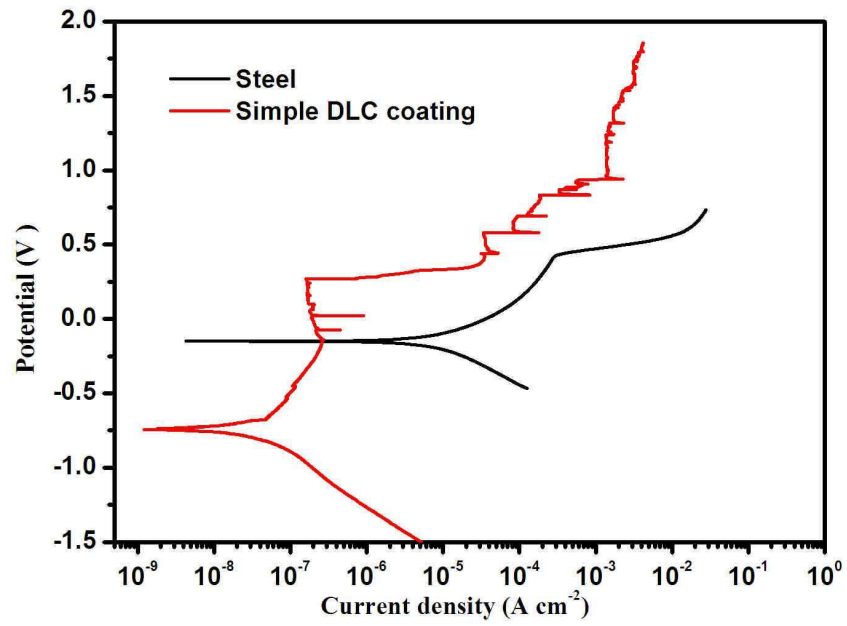


Figure 7

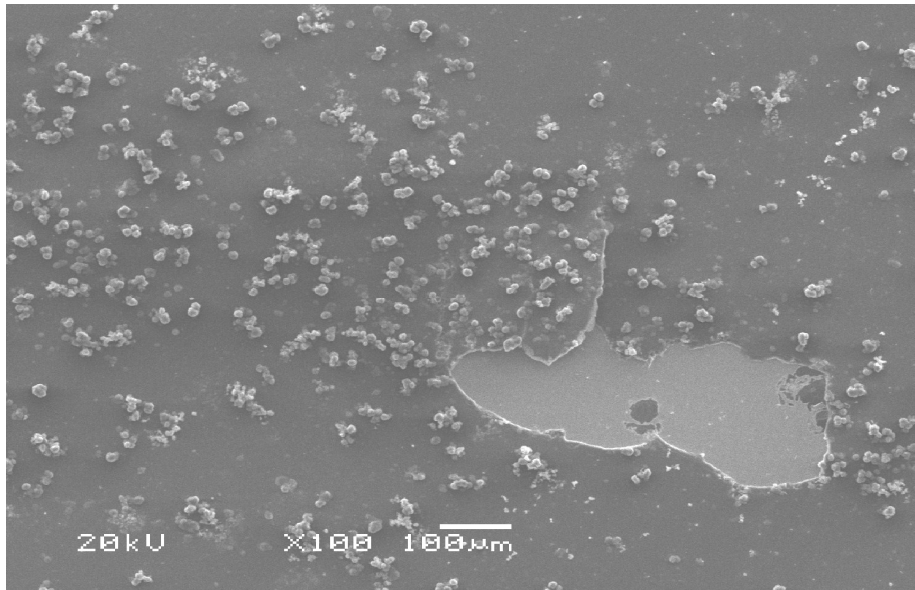


Figure 8

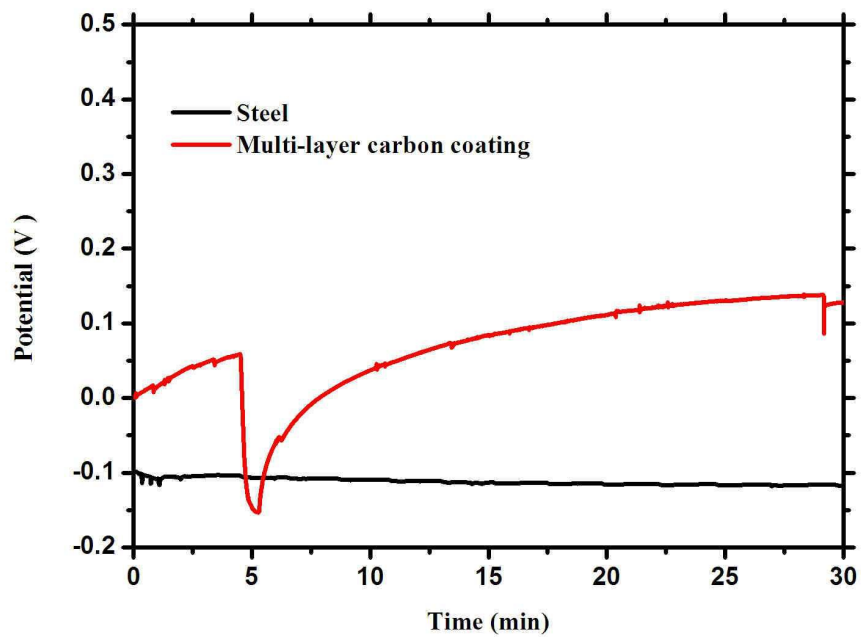


Figure 9

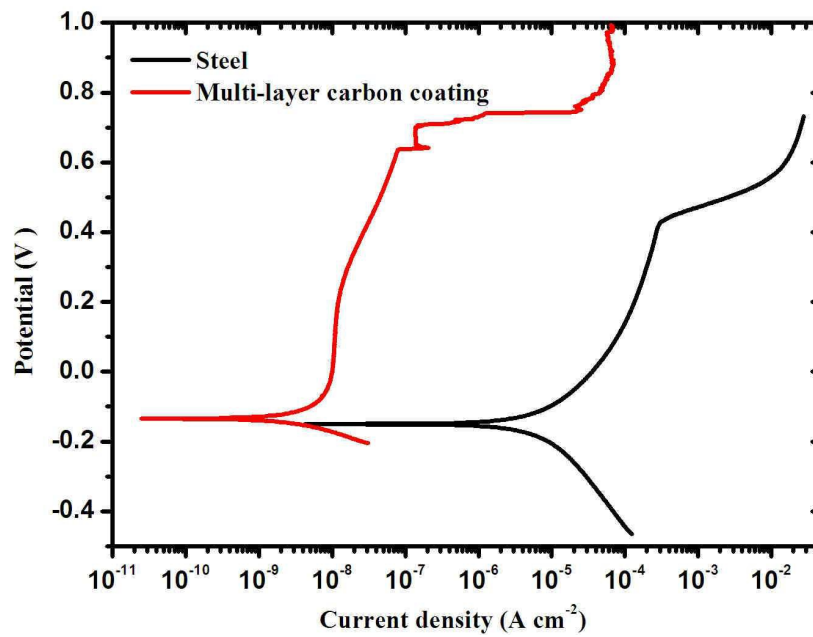


Figure 10

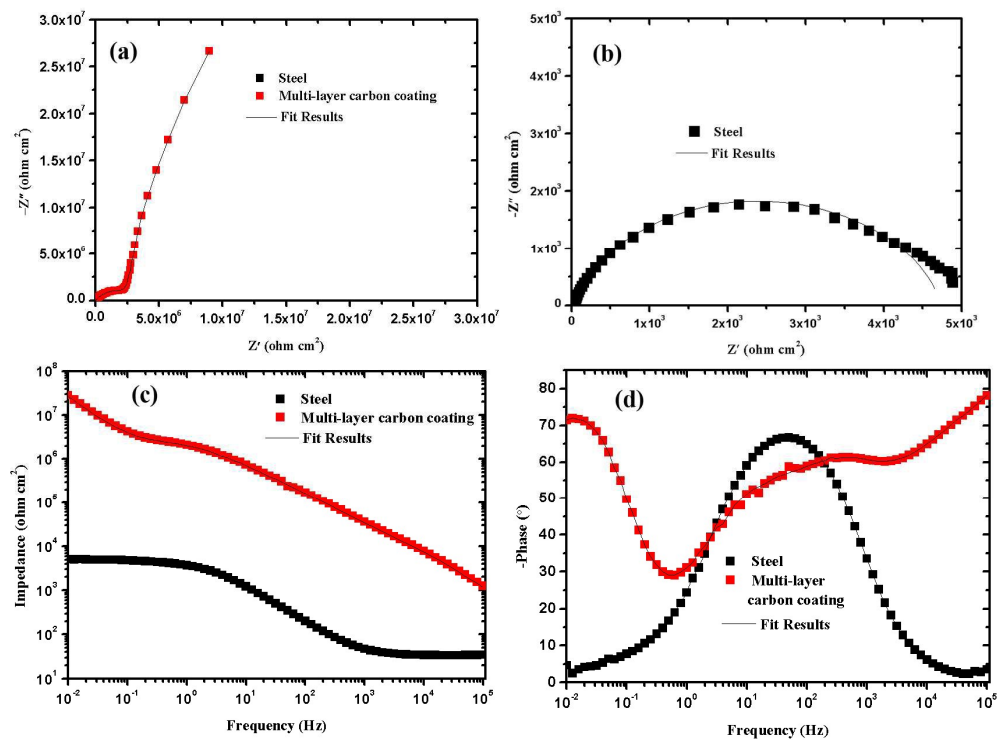


Figure 11

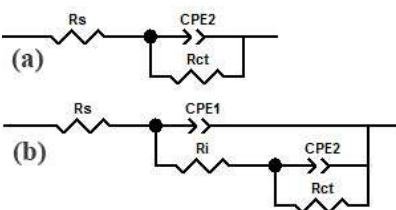


Figure 12

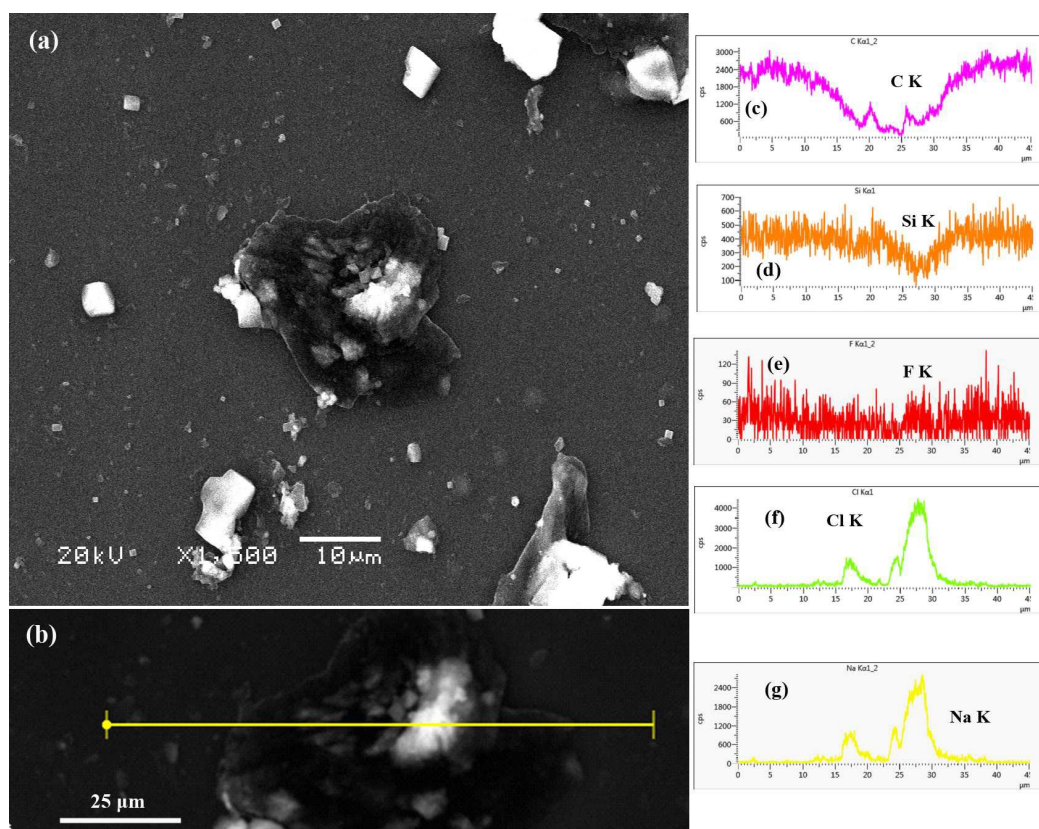


Figure 13

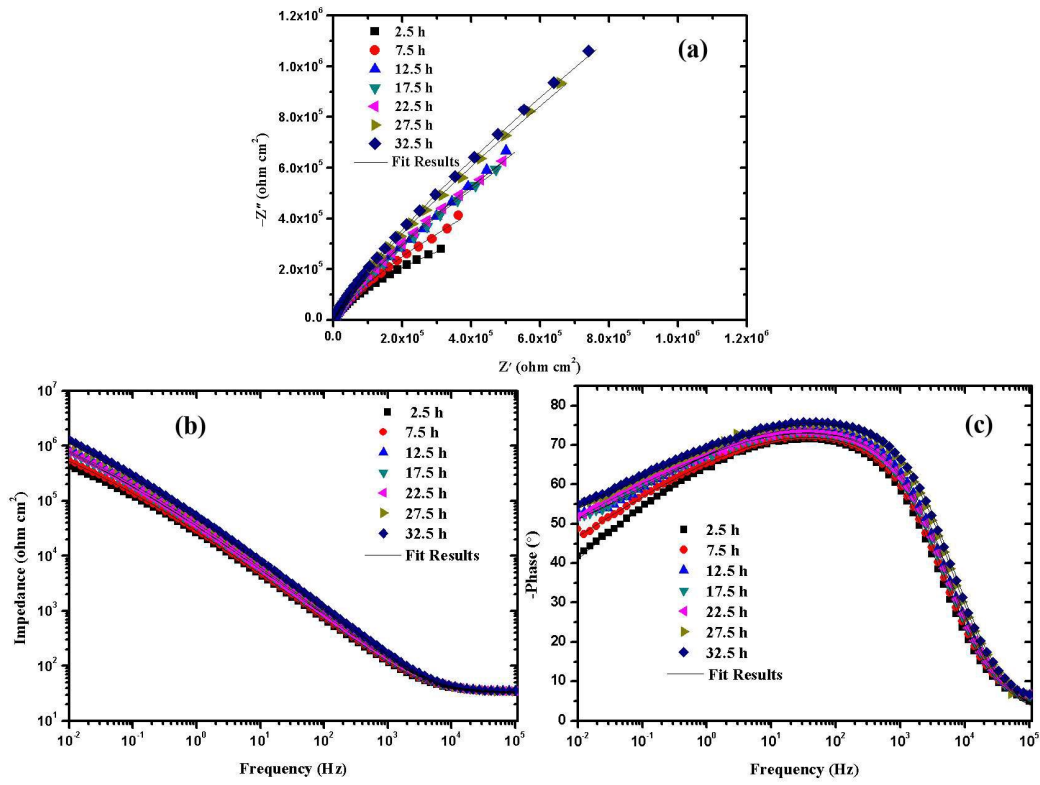


Figure 14

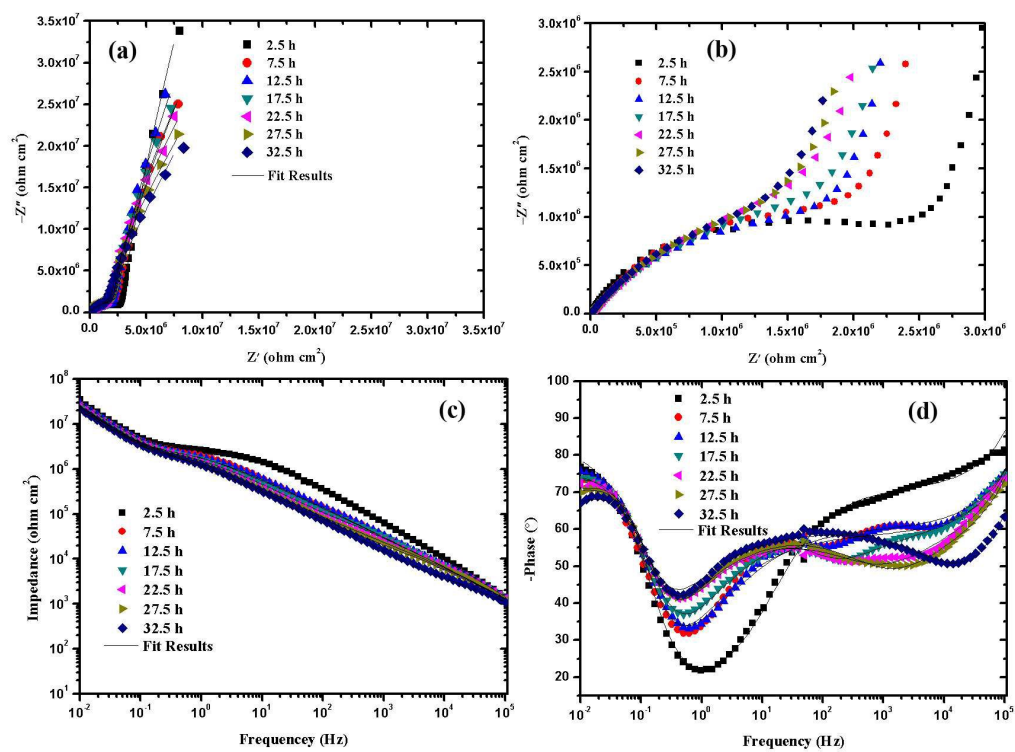


Figure 15

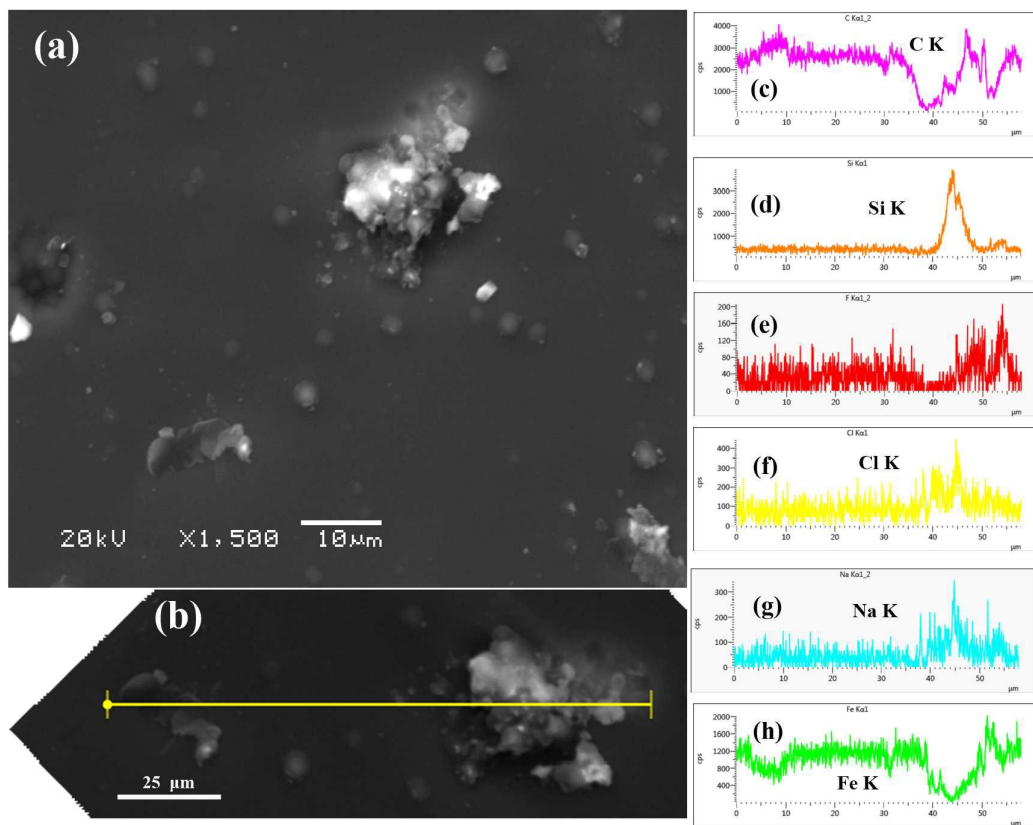


Figure 16

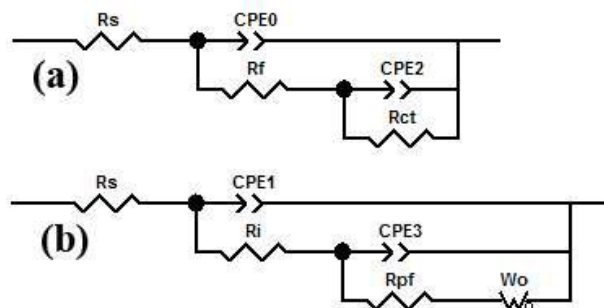


Figure 17

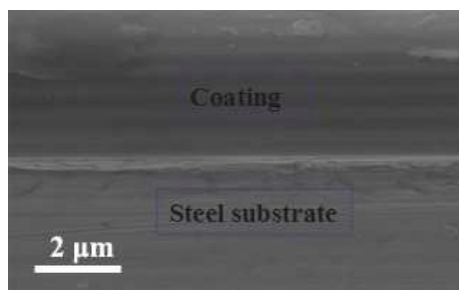


Figure 18

